Motion robust ICG measurements using a two-step spectrum denoising method

Yao Xie[1,3], Rencheng Song[2], Dong Yang[3], Honglong Yu[2], Cuimin Sun[1], Qilian Xie[3,4] and Ronald X. Xu[1]

[1] School of Engineering Science,University of Science and Technology of China, Hefei, 230027,China

[2] Department of Biomedical Engineering, Hefei University of Technology, Hefei, 230009, China

[3] Anhui Tongling Bionic Technology Co. Ltd, No. 5089, Wangjiang West Road, Hefei, China

[4] Anhui Medical University, Hefei, 230032, China

E-mail: rcsong@hfut.edu.cn

Abstract. *Objective.* Impedance cardiography (ICG) is a noninvasive and continuous method for evaluating stroke volume and cardiac output. However, the ICG measurement is easily interfered due to respiration and body movements. Taking into consideration about the spectral correlations between the simultaneously collected ICG, electrocardiogram (ECG), and acceleration signals, this paper introduces a two-step spectrum denoising method to remove motion artifacts of ICG measurements in both resting and exercising scenarios. *Approach.* First, the major motion artifacts of ECG and ICG are separately suppressed by the spectral subtraction with respect to acceleration signals. The obtained ECG and ICG are further decomposed into two sets of intrinsic mode functions (IMFs) through the ensemble empirical mode decomposition (EEMD). We then extract the shared spectral information between the two sets of IMFs using the canonical correlation analysis (CCA) in a spectral domain. Finally, the ICG signal is reconstructed using those canonical variates with largest spectral correlations with ECG IMFs. *Main results.* The denoising method was evaluated for 30 subjects under both resting and cycling scenarios. Experimental results show that the beat contribution factor of ICG signals increases from its original 80.1% to 97.4% after removing the motion artifacts. *Significance.* The proposed denoising scheme effectively improves the reliability of diagnosis and analysis on cardiovascular diseases relying on ICG signals.

Keywords: impedance cardiography (ICG), motion artifacts, spectral subtraction, ensemble empirical mode decomposition (EEMD), canonical correlation analysis (CCA).

1. Introduction

Stroke volume (SV) refers to the volume of blood ejected from the ventricle in one cardiac cycle (Guyton 1986). Cardiac output (CO), which is obtained by multiplying SV with heart rate, represents the amount of blood ejected from the heart in one minute (Kubicek et al. 1974). The noninvasive and continuous estimation of SV and CO during exercise is particularly useful in the evaluation of patients with cardiovascular diseases such as heart failure, aortic stenosis, coronary heart disease, and other valvular diseases (Kim et al. 1992, Zhang et al. 2007).

Three typical methods of measuring SV are the Fick formula, dye dilution, and thermodilution (Yakimets & Jensen 1995). However, these methods are in general invasive and noncontinuous, and thereby limiting their usage in many patients (Kubicek et al. 1974). Esophageal echocardiography and Doppler echocardiography are common noninvasive methods for measuring SV (Naidu et al. 2015, Revzin et al. 2017). But these measurements are also noncontinuous, and the results are highly dependent on the operator's experience (Revzin et al. 2019). In contrast, impedance cardiography (ICG) is a noninvasive and continuous method to estimate SV and CO (Kubicek et al. 1974, Sherwood et al. 1990, Anand et al. 2021). It monitors the thoracic impedance and correlates impedance variation with various events in the cardiac cycle. The ICG injects a high-frequency low-amplitude constant current into the thorax through two electrodes. Another pair of electrodes placed on the boundary of the current injecting electrodes are used to measure the thoracic voltage. Finally, the time-varying impedance signal is obtained through Ohm's law, and the negative of the impedance signal derivative is called the ICG (Bagal et al. 2017).

The measurement of SV and CO depends on the accurate identification of the characteristic points in the ICG waveform. As shown in Figure 1, the critical characteristic points include B, C, and X, which represent the opening of the aortic valve, the maximum ejection velocity, and the closing of the aortic valve, respectively (Choudhari & Panse 2014). However, the detection of these reference points becomes more challenging, when displacements of electrodes are caused by body movements and respiration (Sherwood et al. 1990).

There are several signal processing methods for removing motion artifacts from ICG recordings. For example, the band-pass filtering can remove noise components outside the frequency band (Yamamoto et al. 1988, Raza et al. 1992). But it has limitation to deal with artifacts with the spectrum overlapped with the target signal. Another frequently used method, the adaptive filtering, can update the filter weights automatically to fit the input noise level (Rosell et al. 1995, Alexander 2012, Hu et al. 2014, Mallam & Rao 2016). While researchers have presented analyses of ICG using adaptive filtering techniques, it is generally difficult to identify the filter weights related to the sources of various artifacts (Choudhari & Panse 2014). Wavelet transform is a time-scale representation of a digital signal and has been widely used in ICG signal denoising (Pandey & Pandey 2007, Sebastian et al. 2011, Chabchoub

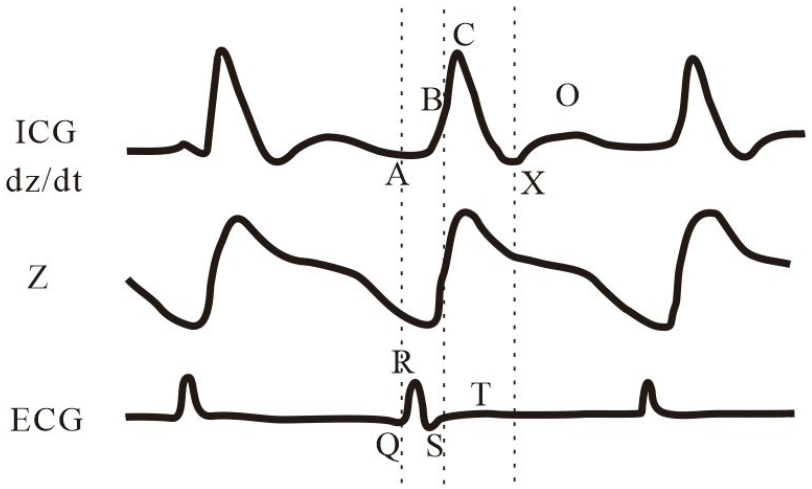

Figure 1. The characteristic relationship diagram between ICG and ECG signals.

et al. 2016, Stepanov et al. 2017). The challenge of wavelet-based methods is to select the optimal mother wavelet, since it strongly affects the denoising effects (Ngui et al. 2013). Ensemble averaging is performed by totaling up the digitized samples of each signal and dividing by the number of synchronized beats on average, thereby reducing the impact of single-beat fluctuations in the impedance signal (Muzi et al. 1985, Riese et al. 2003, Ishiguro et al. 2006, Sheikh et al. 2020). Although this method can eliminate artifacts in emotional tension or slight shaking, it is not effective in removing motion artifacts under conditions with intense exercise.

Considering the spectral correlations between the simultaneously collected ICG, the electrocardiogram (ECG), and the acceleration signals, this paper proposes a two-step spectrum denoising method to remove motion artifacts in ICG signals with respect to the ECG and acceleration signals. First, the spectral subtraction technique (Zhang et al. 2014, Arunkumar & Bhaskar 2020) is used to remove major motion artifacts caused by body movements in ICG and ECG regarding the acquired acceleration signals. On the other hand, since the ECG and ICG signals have strong correlations in the frequency domain due to synchronized heart rhythm, the ICG can be further denoised using the spectral correlation with ECG. Accordingly, the single-channel ICG and ECG signals are decomposed respectively into intrinsic mode functions (IMFs) by the ensemble empirical mode decomposition (EEMD). The canonical correlation analysis (CCA) (De Clercq et al. 2006, Sweeney et al. 2012, Chen et al. 2017) is then taken to determine the shared components between spectra of the two IMF sets. Finally, the denoised ICG signal is reconstructed by removing those spectral components with low correlations, thereby indirectly removing motion artifacts. We test the denoising method for 30 subjects under both resting and cycling scenarios. Experimental results demonstrate clear enhancements on the quality of ICG signals after removing the motion artifacts. The proposed denoising scheme provides an efficient way of measuring stable ICG, especially under exercising scenarios, which improves the reliability of follow-up diagnosis and

analysis relying on ICG signals.

2. Method

2.1. Dataset

The in-house dataset collects ECG, ICG, and acceleration signals from 30 subjects (15 women and 15 men, whose age ranges between 21 to 45) under the resting and exercising scenarios, respectively. All signals last a total of 150 seconds. As shown in Figure 2, the participants were seated in an armchair (30 seconds) for the resting case and they rode on a spinning bike (120 seconds) for the exercising case during recording. The positions of the ICG electrodes, ECG electrodes and accelerometer are marked in Figure 2(b) with red, orange and green boxes, respectively. The experimental procedures were approved by the Ethics Committee in Human Research of the University of Science and Technology of China. Prior to the collection of the data, all the volunteers filled out an informed consent form.

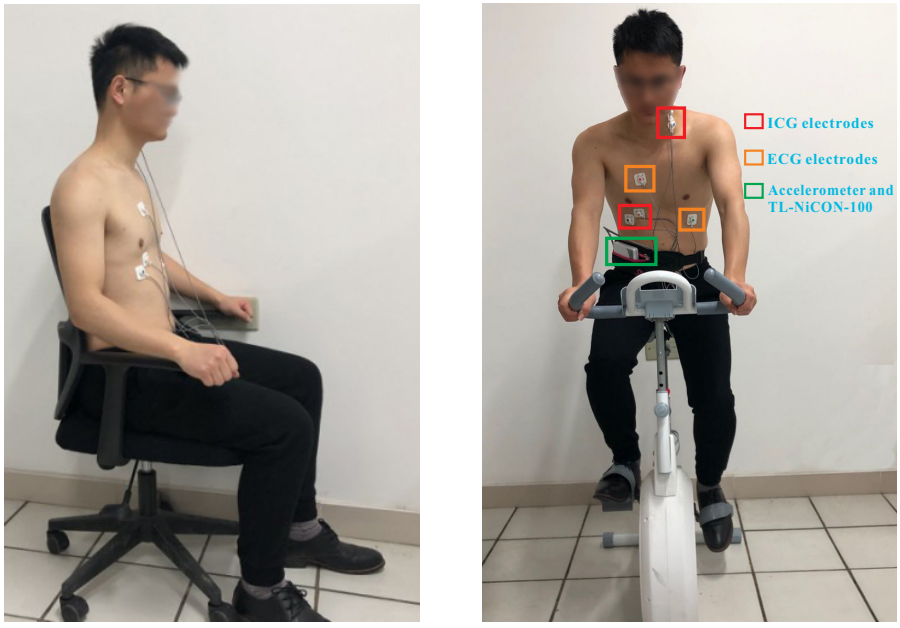

(a) resting period (b) cycling period

Figure 2. A data collection example for recording the subjects' ICG, ECG, and acceleration signals under two scenarios.

The ICG, ECG, and acceleration signals were obtained simultaneously through a physiological signal module TL-NiCON-100 (Anhui Tongling Bionic Technology Co., Ltd.) and transmitted wirelessly to a laptop using a 200 Hz sampling rate. According to the description of Kubicek et al., the ICG signal is obtained by a classic tetrapolar array, placing the current electrode around the bottom of the neck and the ground electrode near the thorax 3 cm below the xiphisternal junction. The remaining two electrodes are voltage electrodes, and they are 3 cm away from the current electrode

Figure 3. The flowchart of the proposed method for removing motion artifacts in ICG signals.

and the ground electrode. The injected current was set at 2mA and 50 kHz. The ECG signal was obtained by two more electrodes following the Lead II array. The two active electrodes were placed on the centerline of the right clavicle and the sixth rib of the left midclavicular line. The ground electrode was shared with the ICG signal. All electrodes were provided by 3M company. The accelerometer sensor was integrated into the TL-NiCON-100, which can collect acceleration signals in x, y, and z directions in real time. TL-Analysis-Software was used to store, display, and export the data in CSV format. Further analysis and development of the algorithm were carried out in MATLAB R2016a (MathWorks Inc. Natick, Mass.).

2.2. Algorithm Implementation

The flowchart of the algorithm is depicted in Figure 3, which includes five steps: preprocessing, spectral subtraction, EEMD, CCA in spectrum domain, and reconstruction. The preprocessing performs bandpass filtering on physiological signals

Algorithm 1 Denoising algorithm of ICG signals

1: Slice the ECG, ICG, and acceleration signals into segments. Filter the ECG and ICG signals with a bandpass filter [0.7 25.0] Hz and [0.7 6.0] Hz, respectively. Use acceleration signals to fuse the motion signal.
2: Normalize the spectrum of ICG, ECG, and the motion signal, then perform spectral subtraction for ICG and ECG separately.
3: Decompose the processed ECG and ICG from single-channel signals into multi-channel signals (IMFs) by EEMD. Selects IMFs with a dominant frequency falling into [0.7 6.0] Hz. The spectra of N selected IMFs are calculated by the fast Fourier transform (FFT), which are denoted as vectors $\mathbf{s}_{1,ICG}, ..., \mathbf{s}_{N,ICG}$ and $\mathbf{s}_{1,ECG}, ..., \mathbf{s}_{N,ECG}$. Set the matrices $\mathbf{S}_{ICG} = [\mathbf{s}_{1,ICG}, ..., \mathbf{s}_{N,ICG}]^T$, and $\mathbf{S}_{ECG} = [\mathbf{s}_{1,ECG}, ..., \mathbf{s}_{N,ECG}]^T$.
4: Take CCA on $\mathbf{S}_{ICG}$ and $\mathbf{S}_{ECG}$. Suppose the canonical variates (CVs) of ICG and ECG are denoted as matrices $\mathbf{U}_{ICG}$ and $\mathbf{V}_{ECG}$, respectively, while the corresponding canonical correlation coefficient vector is $\mathbf{r} = [r_1, r_2, ..., r_k, ..., r_N]$.
5: Set the $\mathbf{U}_{ICG}(i, :) = 0$ if the $i > 1$ & $\mathbf{r}(i) < 0.9$.
6: Reconstruct the ICG with retained CVs and obtain the final denoised ICG.

and fuses motion signals. Spectral subtraction aims to suppress the major motion artifacts in ICG and ECG. The EEMD is taken to decompose the single-channel physiological signals into multi-channel IMFs, while the CCA is used to obtain the most relevant part between the spectra of two IMF sets. Finally, the reconstruction module obtains the denoised ICG signal through eliminating those canonical variates with low correlations in the spectrum domain. The whole denoising method is summarized in Algorithm 1 and detailed implementations are introduced as below.

2.2.1. Preprocessing The ECG, ICG, and acceleration signals are respectively sliced into non-overlapping segments. There are total of 30 subjects, and each subject records data of 150 seconds, which is further cut into segments of 10 seconds. Therefore, there are 450 segments (30(*subject*)*150(*s/subject*)/10(*s/segment*)), including 90 in resting periods and 360 in cycling periods. Most of the content of the ICG signal is in the band of [0.5 4.0] Hz (Liu et al. 2018, Muñoz et al. 2018). Taking into account the increase in HR during exercise, the fundamental of the ICG spectrum will move forward. Therefore, the cutoff frequency is set as [0.7 25.0] Hz for ECG signal, and [0.7 6.0] Hz for the ICG signal and acceleration signals. The fast Fourier transform (FFT) is applied to the acceleration signals in x, y and z directions, and the obtained amplitudes are labeled as $\mathbf{s}_{\mathrm{x}}$, $\mathbf{s}_{\mathrm{y}}$ and $\mathbf{s}_{\mathrm{z}}$, respectively. As shown in Eq. 1, we select the maximam magnitude of the three frequency spectra for each frequency bin that can most effectively represent the motion artifacts (Tariqul Islam et al. 2018)

$$\mathbf{s}_{\mathrm{M}}(k) = \max(\mathbf{s}_{\mathrm{x}}(k), \mathbf{s}_{\mathrm{y}}(k), \mathbf{s}_{\mathrm{z}}(k)), \tag{1}$$

where $\mathbf{s}_{\mathrm{M}}(k)$ is the spectrum of motion signal, and k is the index of spectral components.

2.2.2. Spectral Subtraction The spectral subtraction is a technique used to remove major motion spectra from the spectra of physiological signals (Zhang et al. 2014). In this paper, the term spectrum subtraction refers to magnitude spectrum subtraction. Suppose $\mathbf{s}_{\mathrm{P}}(k)$ denotes the normalized spectrum of ICG or ECG signal and $\mathbf{s}_{\mathrm{a}}(k)$ is the normalized spectrum of motion of $\mathbf{s}_{\mathrm{M}}(k)$. A generalized spectral subtraction performs the following operations,

$$|\mathbf{s}(k)| = \begin{cases} |\mathbf{s}_{\mathrm{P}}(k)| - |\mathbf{s}_a(k)|, & |\mathbf{s}_{\mathrm{P}}(k)|>|\mathbf{s}_a(k)| \ \&\ k \neq f_{hr} \\ |\mathbf{s}_{\mathrm{P}}(k)|, & k = f_{hr} \\ 0, & \text{otherwise} \end{cases} \tag{2}$$

where $\mathbf{s}(k)$ is the spectrum of ICG or ECG after spectrum subtraction, k is the index of spectral components, and f_{hr} is the estimated frequency of heart rate (HR) by ECG. As shown in Eq.2, $\mathbf{s}(k)$ is set to zero when the motion spectrum component is higher than the spectrum of ICG or ECG, which is to avoid negative spectrum peak after spectral subtraction. Particularly, this method prevents the HR component from being weakened during the spectral subtraction process if peaks of motion artifacts are close to true HR peak.

2.2.3. EEMD-CCA in spectrum domain The spectral subtraction can only remove major motion artifacts from the ICG and ECG signals. Considering its spectrum correlation with ECG, we take the CCA to further enhance the quality of ICG signal. As required by CCA, the single-channel ECG and ICG need to be decomposed into multi-channel signal sets. Here the EEMD is used to decompose the physiological signals into intrinsic mode functions (IMFs). The algorithms of EEMD and the following CCA in spectrum domain are introduced as below.

EEMD is a noise-assisted data analysis method aimed at overcoming the mode mixing deficiencies of the empirical mode decomposition (EMD). To do this, each signal in EEMD is consisted of the original signal plus a finite amplitude white noise (Wu & Huang 2009, Motin et al. 2016). The EEMD then defines the IMFs as the mean of an ensemble of trials. Accordingly, the preprocessed physiological signal $\mathbf{p}(t)$ (ICG or ECG after spectral subtraction) is added with white noise $\mathbf{n}(t)$ to generate a new signal $\mathbf{q}(t)$ (Eq. 3), which is decomposed into IMFs (Eq. 4),

$$\mathbf{q}(t) = \mathbf{p}(t) + \alpha\mathbf{n}(t), \tag{3}$$

$$\mathbf{q}(t) = \sum_{i=1}^{K} \mathbf{z}_i(t) + \mathbf{r}_n(t), \tag{4}$$

where $\mathbf{z}_i$ is the ith IMF, K is total number of obtained IMFs, α is the magnitude of the white noise, and $\mathbf{r}_n$ is the residual signal after EEMD. The obtained IMFs are sorted by their dominant frequencies. We only keep the IMFs with a dominant frequency within [0.7 6] Hz. To guarantee the performance of the subsequent CCA processing, we choose the channel number of selected IMFs to be at least five. If the actual number of selected IMFs is less than five, we will also retain neighboring IMFs as a supplement.

The spectra of selected IMFs are calculated by the fast Fourier transform (FFT), which are denoted as vectors $\mathbf{s}_{1,ICG}, ..., \mathbf{s}_{N,ICG}$ and $\mathbf{s}_{1,ECG}, ..., \mathbf{s}_{N,ECG}$, respectively, where $N \leq K$ is the number of selected IMFs.

Define $\mathbf{S}_{ICG} = [\mathbf{s}_{1,ICG}, ..., \mathbf{s}_{N,ICG}]^T$ and $\mathbf{S}_{ECG} = [\mathbf{s}_{1,ECG}, ..., \mathbf{s}_{N,ECG}]^T$. The CCA is further taken to extract relevant frequency components from $\mathbf{S}_{ICG}$ and $\mathbf{S}_{ECG}$. Accordingly, the canonical variates (CVs) $\mathbf{u}_{ICG}$ and $\mathbf{v}_{ECG}$ can be represented as $\mathbf{u}_{ICG} = \mathbf{w}_1^T * \mathbf{S}_{ICG}$ and $\mathbf{v}_{ECG} = \mathbf{w}_2^T * \mathbf{S}_{ECG}$, where $\mathbf{w}_1$ and $\mathbf{w}_2$ are the weight vectors, respectively (De Clercq et al. 2006). The objective function of CCA is defined as

$$\max_{\mathbf{w}_1, \mathbf{w}_2} r(\mathbf{u}_{ICG}, \mathbf{v}_{ECG}) = \frac{\mathbf{w}_1^T \mathbf{\Sigma}_{12} \mathbf{w}_2}{\sqrt{\mathbf{w}_1^T \mathbf{\Sigma}_{11} \mathbf{w}_1} \sqrt{\mathbf{w}_2^T \mathbf{\Sigma}_{22} \mathbf{w}_2}}, \tag{5}$$

where r indicates the canonical correlation coefficient, $\mathbf{\Sigma}_{11}$ and $\mathbf{\Sigma}_{22}$ are the auto-covariance matrices of $\mathbf{S}_{ICG}$ and $\mathbf{S}_{ECG}$, respectively, and $\mathbf{\Sigma}_{12}$ is cross-covariance matrix of $\mathbf{S}_{ICG}$ and $\mathbf{S}_{ECG}$. Suppose we get N CVs with canonical correlation coefficients denoted as a vector $\mathbf{r} = [r_1, r_2, ..., r_k, ..., r_N]$. For obtaining the Mth ($M \leq N$) r_M value, it is also calculated by Eq. 5. However, the Mth pair canonical variates $(\mathbf{u}_{ICG,M}, \mathbf{v}_{ECG,M})$ is further required to be uncorrelated with the obtained canonical variables $(\mathbf{u}_{ICG,1}, \mathbf{v}_{ECG,1})$, $(\mathbf{u}_{ICG,2}, \mathbf{v}_{ECG,2})$, ..., $(\mathbf{u}_{ICG,M-1}, \mathbf{v}_{ECG,M-1})$ at the same time. The total N CVs for ICG and ECG are recorded in matrices $\mathbf{U}_{ICG}$ and $\mathbf{V}_{ECG}$, respectively. The corresponding weight vectors are stored in matrices $\mathbf{A}_{ICG}$ and $\mathbf{B}_{ECG}$, respectively.

Because the ICG and ECG have strong correlations on the spectrum components, the canonical variate $\mathbf{u}_{ICG}$ for ICG with a correlation coefficient $\mathbf{r}$ satisfied $i > 1$ & $\mathbf{r}(i) < 0.9$ is considered as an artifact, which will be set to zero before reconstructing the ICG signal.

2.2.4. Reconstruction of the ICG Signal As given in Eq. 6, the ICG spectrum set can be reconstructed by the retained canonical coefficients $\tilde{\mathbf{A}}_{ICG}$ and the corresponding canonical scores $\tilde{\mathbf{U}}$ as

$$\tilde{\mathbf{S}}_{ICG} = \tilde{\mathbf{A}}_{ICG}^{-1} \tilde{\mathbf{U}}_{ICG}, \tag{6}$$

where $\tilde{\mathbf{S}}_{ICG} = [\tilde{\mathbf{s}}_{1,ICG}, ..., \tilde{\mathbf{s}}_{N,ICG}]^T$ is the reconstructed ICG spectrum set and $\tilde{\mathbf{s}}_{i,ICG}$ is the denoised spectrum of ith ICG IMF.

Therefore, the ith denoised IMF $\tilde{\mathbf{z}}_{i,ICG}$ of ICG in time domain is then easily determined by the inverse Fourier transform with the spectrum $\tilde{\mathbf{s}}_{i,ICG}$ and corresponding phase information,

$$\tilde{\mathbf{z}}_{i,ICG}(n) = \frac{1}{M} \sum_{k=0}^{M-1} \tilde{\mathbf{s}}_{i,ICG}(k) \exp(jnk\frac{2\pi}{M}), i = 1, 2, \ldots, N \tag{7}$$

where M is the number of points for inverse Fourier transform.

Finally, we add up all the obtained ICG IMFs as below,

$$\mathbf{ICG}(n) = \sum_{i=1}^{N} \tilde{\mathbf{z}}_{i,ICG}(n), \tag{8}$$

Algorithm 2 Detection of ICG characteristic points

1: Detect the R and Q characteristic points from ECG.
2: Scan the ICG segment from the range of ECG R-peak to R-peak + RR-interval/3. Find the maximum point (dz/dt_{max}) as the C point (Forouzanfar et al. 2018).
3: Find the point B as the one which is closest to 0.15*dz/dt_{max} within the 20% to 65% of the RC interval (Naidu et al. 2011, Bagal et al. 2017).
4: Scan the ICG segment from ECG T-peak to T-peak + RR-interval/3 and mark the obtained minimum value as the X point.
5: Repeat the process until ICG scans to the end of the segment.

where $\mathbf{ICG}(n)$ is the final denoised ICG signal.

2.3. Evaluation method

The signal quality of ICG affects the accuracy of the detection of characteristic points, which in turn influences the accuracy of corresponding physiological parameters. Due to the lack of reference ICG signal, this article evaluates the ICG signal quality indirectly according to the inherent features of the ICG signal, including the valid beat (VB), beat contribution factor (BCF), average correlation coefficient (ACC), the agreement between the interval of ICG CC (two adjacent C points) and ECG RR (two adjacent R points), the coefficient of variability of pre-ejection period (PEP), and the left ventricular ejection time (LVET).

2.3.1. Detection of ICG characteristic points As shown in Figure 1, the main characteristic points of the ICG signal are B, C, and X, while those of ECG are R and Q. The cardiac function parameters measured via ICG include SV, CO, HR, PEP, LVET, and other derived hemodynamic parameters (Kubicek et al. 1974). The time interval between point B and point X is the LVET, the time interval between ECG point Q and ICG point B is the PEP, the amplitude of point C is dz/dt_{max}, and HR is calculated by ECG RR interval or ICG CC interval. SV is generally calculated using the Kubicek equation using two hemodynamic parameters, the LVET and the dz/dt_{max} of ICG. The CO is SV multiplied by HR. The method for detecting characteristic points can be summarized as Algorithm 2.

2.3.2. ICG signal quality evaluation indicators As shown in Table 1, a beat was identified as a valid one in this paper when the following conditions are satisfied. The LVET is in the range of 160 ms to 380 ms, the PEP is in the range of 50 ms to 160 ms, the RR interval is in the range of 330 ms to 2000 ms, and dz/dt_{max} is in the range of 0.2 Ω/s to 3.0 Ω/s (Cybulski et al. 2017). We indicate that the above conditions are necessary but not sufficient. However, these conditions are of great significance in indirectly evaluating ICG signal quality, since these physiological indicators are important features of ICG signals. More explanations about the above parameters are as follows.

Table 1. Valid range of LVET, PEP, RR and $(dz/dt)_{max}$.

Group	LVET (ms)	PEP (ms)	RR (ms)	$(dz/dt)_{max}$ (Ω/t)
Range	160-380	50-160	330-2000	0.2-3.0

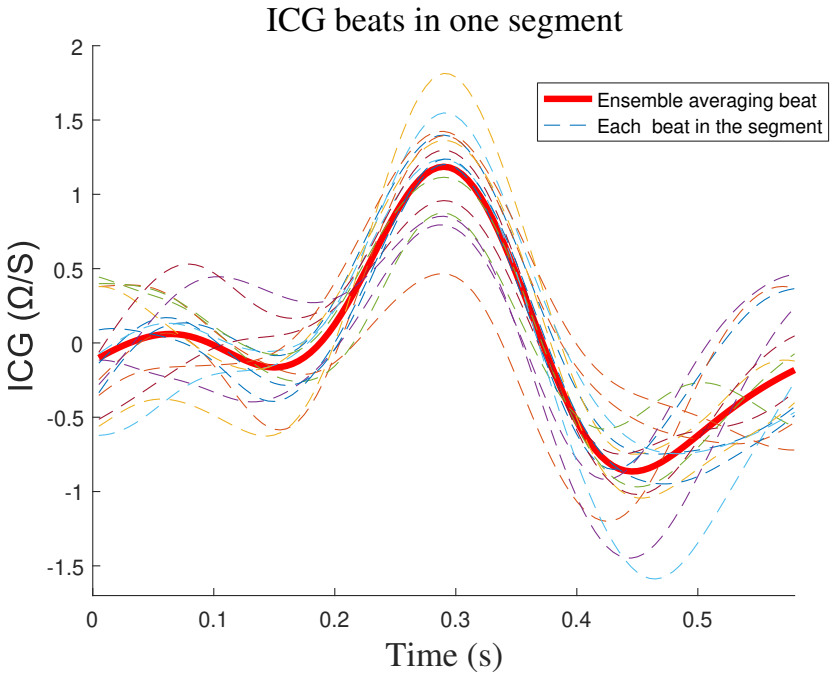

Figure 4. An example of the ensemble averaging beat and single beat in the processing segment.

- The BCF is calculated as the ratio of valid beat number to the total number of beats (Sheikh et al. 2020).
- The ACC is the average value of the correlation coefficients between the ensemble averaging beat and each single beat within the segment. The ensemble averaging beat is the average of each beat in the processing segment as shown in Figure 4. Since each segment lasts for 10 seconds, usually there is little difference between each beat in the segment. Sheikh et al. postulated that normal ACC range is between 0.8 and 1.0, and higher ACC indicates better ICG signal quality (Sheikh et al. 2020).
- The CC interval of ICG is similar to the ECG RR interval, which represents the time interval between two adjacent heartbeats. The CC and RR can both be used to calculate the HR. Considering the correlation of ICG and ECG, the difference between CC and RR can indirectly reflect the quality of the ICG signal. The smaller the difference between CC and RR, the higher the signal quality.
- Finally, the coefficient of variability of hemodynamic parameters (PEP and LVET) in each segment is calculated to assess the quality of the ICG signal. The coefficient of variation indicates the dispersion of measurement, and it is defined as the ratio

of the standard deviation to the mean. The variability of PEP and LVET in each segment is considered to be small within 10 seconds of continuous ICG data. In this article, we assume that the data with a coefficient of variability greater than 15% is abnormal data (Erickson 1986).

3. Results

3.1. Valid Beat and Beat Contribution Factor

Figure 5 shows an example of ICG denoising and the detection of ICG characteristic points under resting and cycling conditions. We normalized the ICG signals to clearly show the difference between the raw ICG and the denoised ICG. As shown, the characteristic points are denoted with different markers, where the denoised ICG signal gets more accurate characteristic points compared with the raw one.

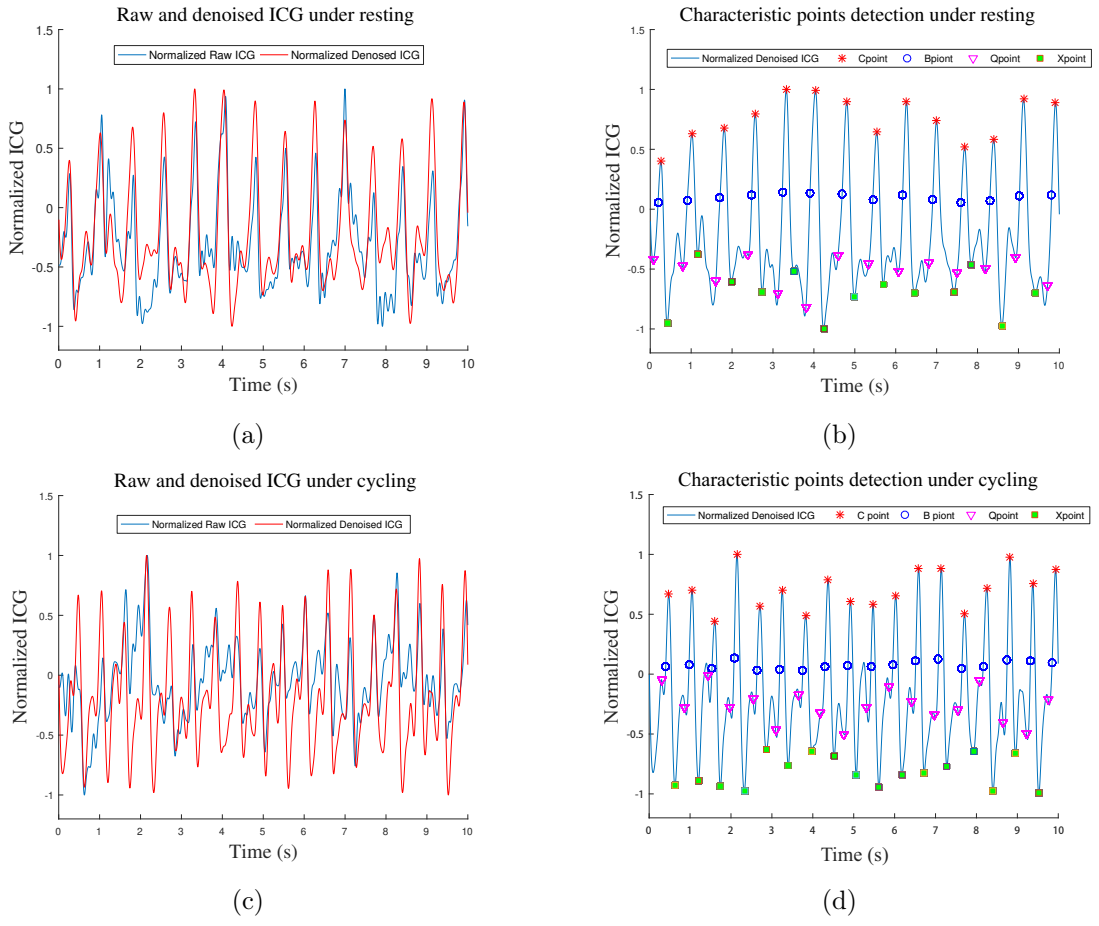

Figure 5. Examples of the ICG denoising and the detection of characteristic points. (a) The effect of ICG denoising in a resting scenario. (b) Detection of ICG characteristic points in a resting scenario. (c) The effect of ICG denoising in a cycling scenario. (d) Detection of ICG characteristic points in a cycling scenario.

The results for all records are summarized in Table 2. In the resting scenario,

Table 2. The comparison of VB and BCF for raw and denoised ICG signals.

Group	VB_{raw}	$VB_{denoised}$	TotalBeat	BCF_{raw}	$BCF_{denoised}$
Resting	976	1049	1068	91.4%	98.2%
Cycling	4773	5942	6108	78.4%	97.3%
All	5749	6991	7176	80.1%	97.4%

there are a total of 1068 beats. After denoising, the number of VB is significantly increased. Meanwhile, the BCF of ICG increases from its original 91.4% to 98.2%. In the cycling scenario, the total beats reach 6108. We have observed similar improvement. Particularly, the BCF of ICG increases from 78.4% to 97.3%. Overall, the average BCF of raw ICG is about 80.1% and that of the denoised one is about 97.4%.

3.2. Average Correlation Coefficient

In the histogram plot shown in Figure 6, the ACC of denoised ICG is significantly higher than those of the raw ICG in all episodes. In the resting period, the ACC of raw ICG ranges from 0.82 to 0.96, and the ACC peak is between 0.95 and 0.96. In contrast, the ACC of denoised ICG ranges from 0.88 to 0.99, and the ACC peak is at 0.97. In the cycling period, the raw ICG has a lower ACC, which ranges from 0.4 to 0.95. Particularly, only 42.5% (153/360) samples exceed 0.8 and 4.4% (16/360) exceed 0.9. It indicates that body movements induced significant noise in the ICG recordings. In comparison, the ACC of denoised ICG ranges from 0.8 to 0.99 with the peak at 0.93. The ACC of all samples exceed 0.8 and about 81.7% (294/360) samples exceed 0.9. It clearly verifies the effectiveness of the proposed denoising algorithm to improve the quality of ICG signals.

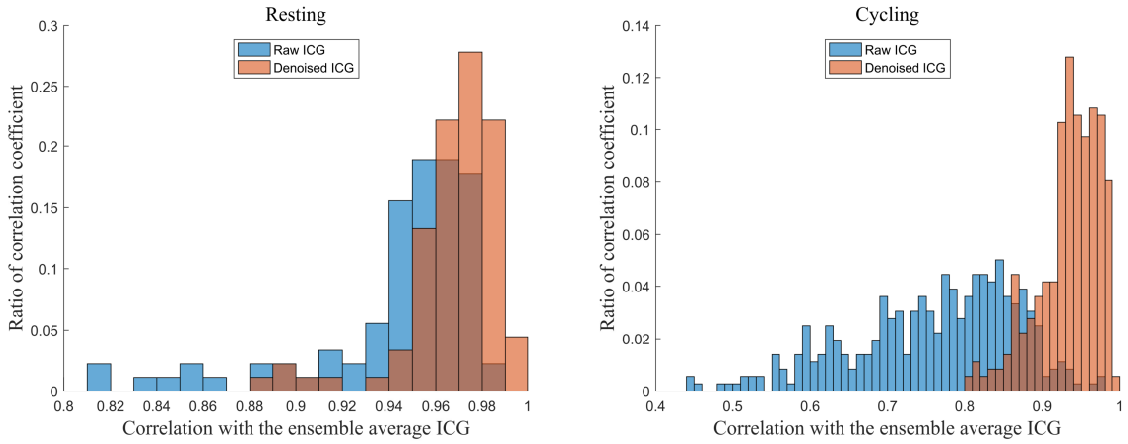

(a) (b)

Figure 6. Average values of correlation coefficients between the ensemble averaging beat and each single beat in the segment. (a) Correlation coefficient in the resting period. (b) Correlation coefficient in the cycling period.

3.3. Agreement between ECG RR Interval and ICG CC Interval

The ECG signal is considered to be less affected by the motion artifacts, so it can be considered as a useful reference for the ICG signal. The Bland-Altman plots in Figure 7 show that there is a large gap between the CC interval of raw ICG and the RR interval of ECG, especially in the cycling period. However, a close agreement between the ECG RR intervals and the denoised ICG CC intervals has been demonstrated after denoising. Compared with the raw ICG, the CC intervals of denoised ICG signals are more consistent with the ECG RR intervals in the overall study (resting and cycling scenarios).

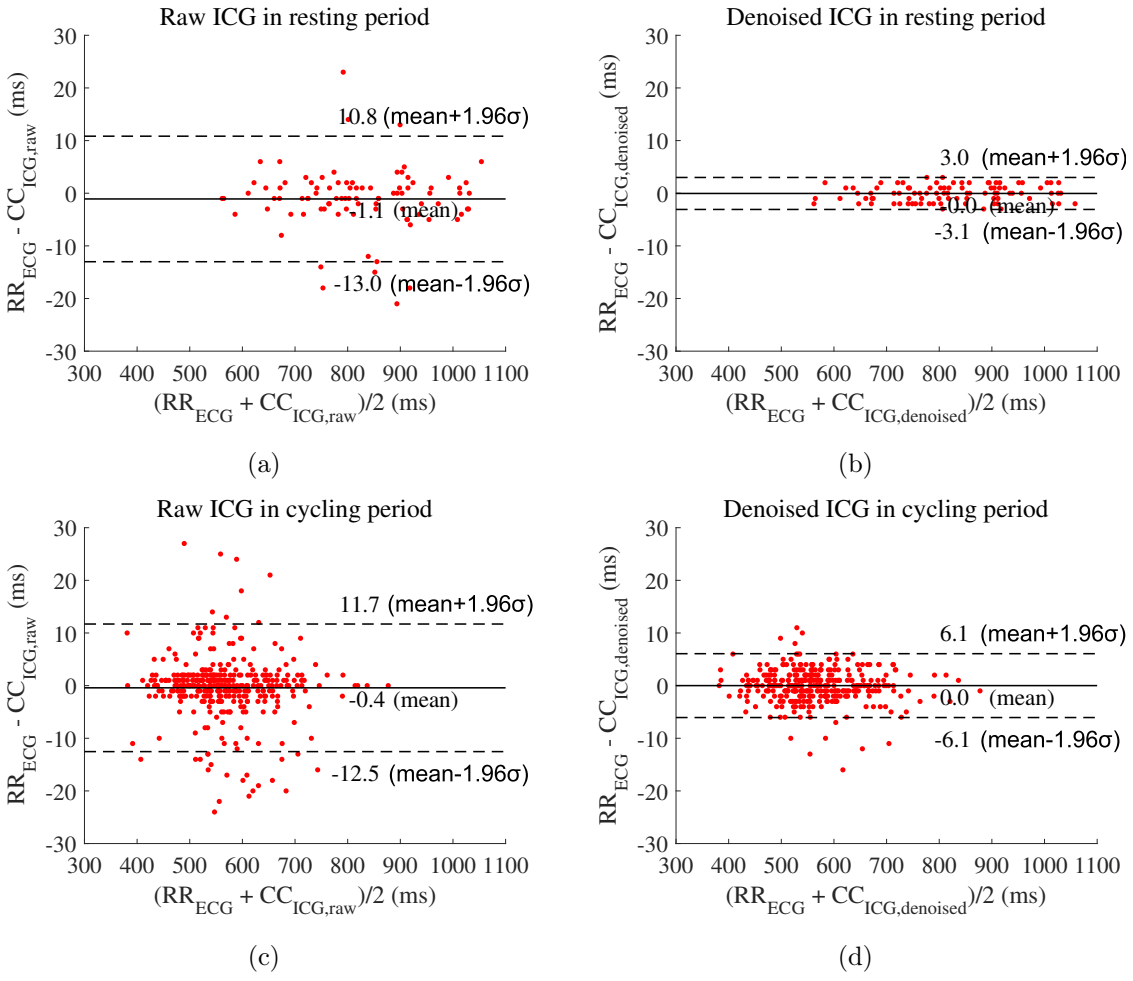

Figure 7. Agreement between the ICG CC intervals and the ECG RR intervals. (a) Bland-Altman plot for raw ICG in the resting period. (b) Bland-Altman plot for denoised ICG in the resting period. (c) Bland-Altman plot for raw ICG in cycling period. (d) Bland-Altman plot for denoised ICG in cycling period.

3.4. Coefficient of Variability of Hemodynamic Parameters

The mean and variance of PEP and LVET are calculated in each segment. The coefficient of variability is used to reflect "intra-subject variability". As shown in Figure 8, the coefficient of hemodynamic parameters (PEP, LVET) variations is significantly lower for denoised ICG signals than that of raw ICG. Particularly, in the resting scenario, the coefficients of variability for the denoised ICG are in general below those of raw ICG signals, and they are almost all below the $y = 0.15 * x$ line. But in the cycling period, only the coefficient of variation of PEP and LVET obtained by denoised ICG are mostly below $y = 0.15 * x$ line.

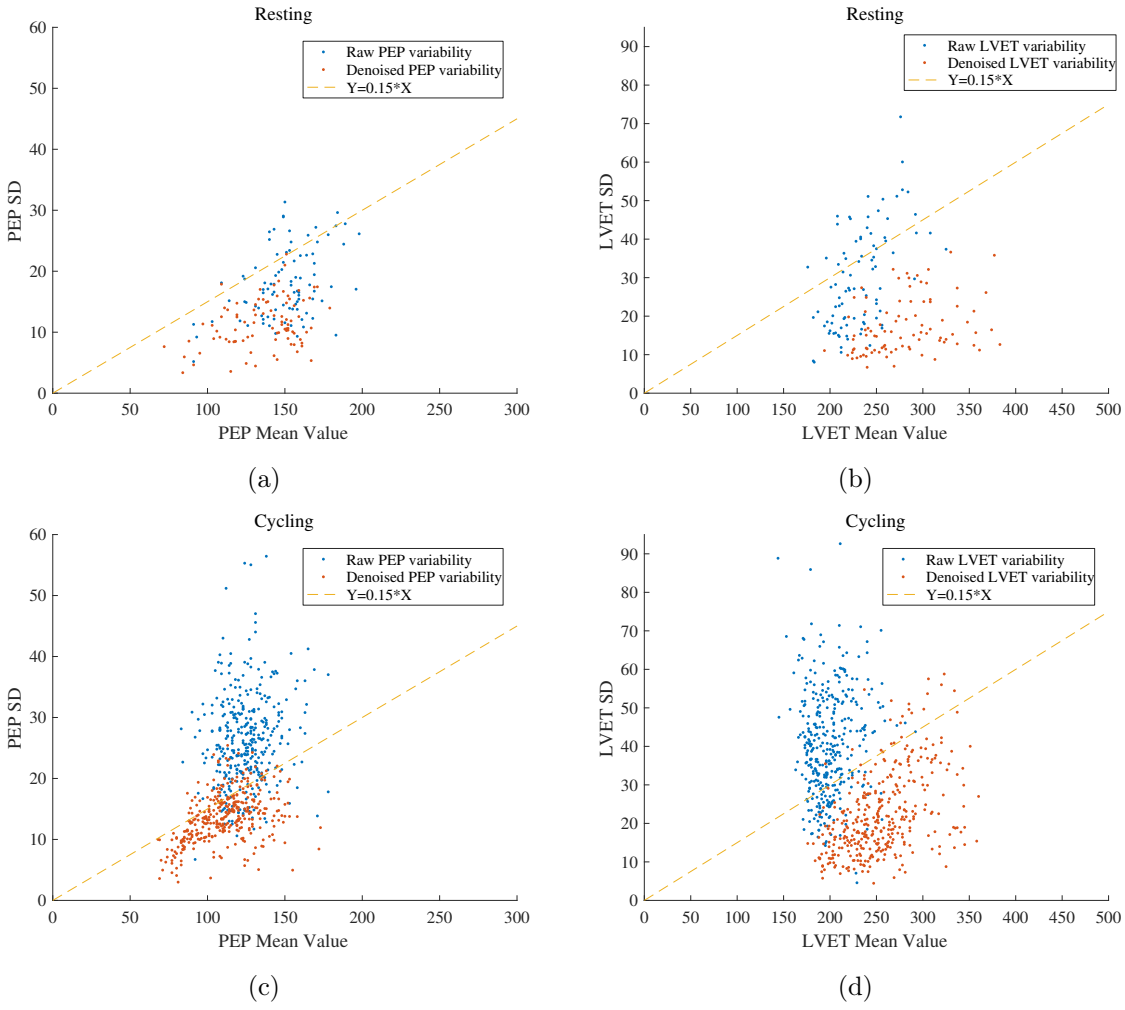

Figure 8. Mean and variance of PEP and LVET in resting and cycling scenarios. (a) Mean and variance of PEP in the resting scenario. (b) Mean and variance of LVET in the resting scenario. (c) Mean and variance of PEP in the cycling scenario. (d) Mean and variance of LVET in the cycling scenario.

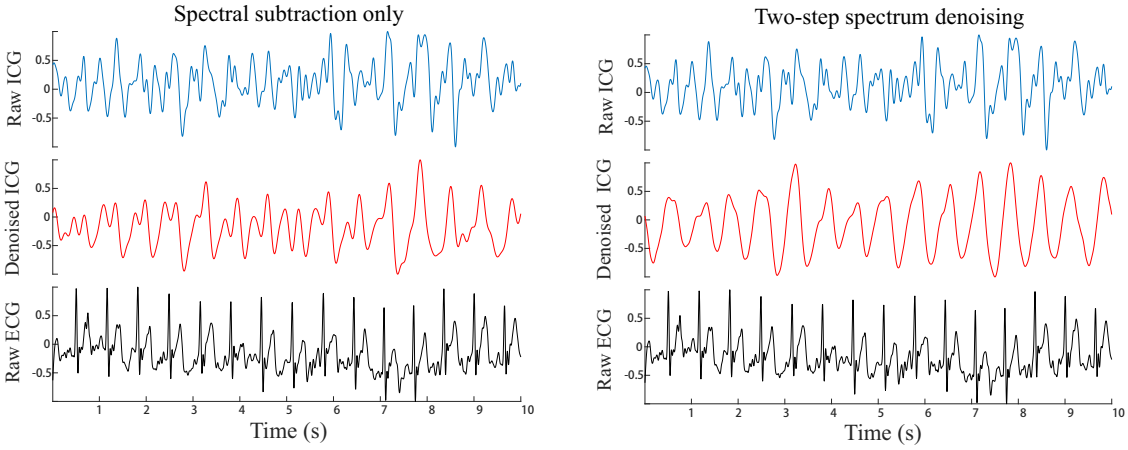

Figure 9. Example results of using only spectral subtraction (left) and the two-step spectrum denoising method (right).

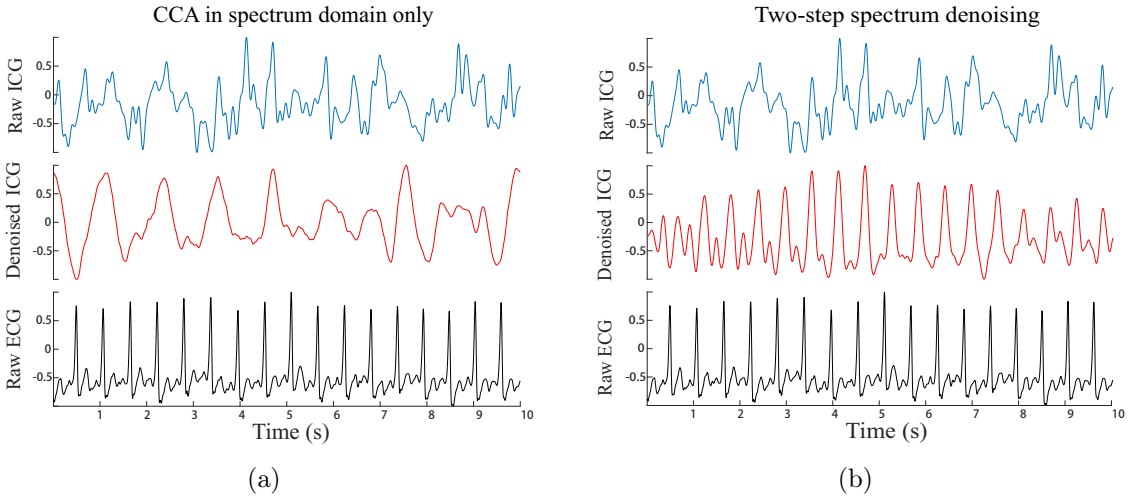

Figure 10. Example results of using only CCA in spectrum domain (left) and the two-step spectrum denoising method (right).

4. Discussion

The above experimental results demonstrate the effectiveness of the proposed method to denoise the ICG signals with motion interference. Ablation study is used to describe the process of removing certain parts of the algorithm in order to better understand the behavior of the algorithm (Meyes et al. 2019). Since the proposed ICG denoising method is a two-step method, we take the ablation study to verify the effectiveness of each step in the method.

The proposed two-step spectrum denoising method including spectrum subtraction as well as CCA in spectrum domain. Particularly, the spectrum subtraction eliminates the major frequency components caused by noise (referred to as motion artifacts in this paper), while the CCA is applied to obtain the most relevant parts of the spectra of the

physiological signal, which further removes motion artifacts. Figure 9 shows the results of using spectrum subtraction alone compared to that of using the two-step spectrum denoising method. Figure 10 shows the results of using CCA in spectrum domain alone compared to that of using the two-step spectrum denoising method. The experimental results in the ablation study show that the proposed two-step method is more efficient to improve the ICG quality than each single step, which confirms the validity of the proposed method for removing motion artifacts.

5. Conclusion

In this study, we have introduced a two-step spectrum processing method to denoise ICG signal. The denoising of ICG would allow for reproducible physiological analysis that is beneficial to the diagnosis of cardiovascular diseases. The method has been evaluated for 30 subjects during a motionless resting period and a cycling period. The experimental results show that the BCF of ICG signal increased from the original 80.1% to 97.4% after removal of the motion artifacts. Compared with the raw ICG, the CC interval of the denoised ICG was more consistent with the RR interval of ECG. The ablation experiment also showed that the spectral subtraction as well as the CCA in spectrum domain are both essential steps for removing artifacts. Although we have evaluated the effectiveness of the proposed method under resting and cycling scenarios, we will further check its validity in more motion scenarios other than cycling in future work.

6. Acknowledgments

This work was supported by the National Key R&D Program of China (Grant No. 2020YFC2004400), and the Fundamental Research Funds for the Central Universities (Grant No. WK5290000001).

References

Alexander, T. S. (2012). *Adaptive signal processing: theory and applications*, Springer Science & Business Media.

Anand, G., Yu, Y., Lowe, A. & Kalra, A. (2021). Bioimpedance analysis as a tool for hemodynamic monitoring: overview, methods and challenges, *Physiological Measurement* **42**(3): 03TR01.

Arunkumar, K. & Bhaskar, M. (2020). Heart rate estimation from wrist-type photoplethysmography signals during physical exercise, *Biomedical Signal Processing and Control* **57**: 101790.

Bagal, U. R., Pandey, P. C., Naidu, S. & Hardas, S. (2017). Detection of opening and closing of the aortic valve using impedance cardiography and its validation by echocardiography, *Biomedical Physics & Engineering Express* **4**(1): 015012.

Chabchoub, S., Mansouri, S. & Salah, R. B. (2016). Impedance cardiography signal denoising using discrete wavelet transform, *Australasian Physical & Engineering Sciences in Medicine* **39**(3): 655–663.

Chen, X., Xu, X., Liu, A., McKeown, M. J. & Wang, Z. J. (2017). The use of multivariate EMD and CCA for denoising muscle artifacts from few-channel EEG recordings, *IEEE Transactions on Instrumentation and Measurement* **67**(2): 359–370.

Choudhari, P. C. & Panse, M. (2014). Artifact removal from the radial bioimpedance signal using adaptive wavelet packet transform, *International Journal of Computational Engineering Research (IJCER)* **4**(7): 2250–3005.

Cybulski, G., Młyńczak, G., Żyliński, M., Strasz, A., Gąsiorowska, A. & Niewiadomski, W. (2017). The quality of automatic artifact identification in ambulatory impedance cardiography monitoring, *EMBEC & NBC 2017*, Springer, pp. 165–168.

De Clercq, W., Vergult, A., Vanrumste, B., Van Paesschen, W. & Van Huffel, S. (2006). Canonical correlation analysis applied to remove muscle artifacts from the electroencephalogram, *IEEE Transactions on Biomedical Engineering* **53**(12): 2583–2587.

Erickson, M. (1986). *Analytical Chemistry of PCBs. 2nd edit*, Lewis Publishers. Chelsea, MI.

Forouzanfar, M., Baker, F. C., Zambotti, M., Mccall, C., Giovangrandi, L. & Kovacs, G. (2018). Toward a better noninvasive assessment of preejection period: A novel automatic algorithm for B-point detection and correction on thoracic impedance cardiogram, *Psychophysiology* **55**(8).

Guyton, A. C. (1986). *Textbook of Medical Physiology 7th edit, 754-62*, Philadelphia: WB Saunders Co.

Hu, X., Chen, X., Ren, R., Zhou, B., Qian, Y., Li, H. & Xia, S. (2014). Adaptive filtering and characteristics extraction for impedance cardiography, *Journal of Fiber Bioengineering and Informatics* **7**(1): 81–90.

Ishiguro, T., Umezu, A., Yasuda, Y., Horihata, S. & Barros, A. K. (2006). Modified scaled fourier linear combiner in thoracic impedance cardiography, *Computers in Biology and Medicine* **36**(9): 997–1013.

Kim, D., Song, C. & Lee, M. (1992). A new ensemble averaging technique in impedance cardiography for estimation of stroke volume during treadmill exercise., *Frontiers of Medical and Biological Engineering: The International Journal of the Japan Society of Medical Electronics and Biological Engineering* **4**(3): 179–188.

Kubicek, W., Kottke, F., Ramos, M. U., Patterson, R., Witsoe, D., Labree, J., Remole, W., Layman, T., Schoening, H. & Garamela, J. (1974). The minnesota impedance cardiograph-theory and applications, *Bio-Medical Engineering* **9**(9): 410–416.

Liu, S. H., Wang, J. J., Su, C. H. & Cheng, D. C. (2018). Improvement of left ventricular ejection time measurement in the impedance cardiography combined with the reflection photoplethysmography, *Sensors* **18**(9).

Mallam, M. & Rao, K. C. B. (2016). Efficient reference-free adaptive artifact cancellers for impedance cardiography based remote health care monitoring systems, *SpringerPlus* **5**(1): 1–17.

Meyes, R., Lu, M., de Puiseau, C. W. & Meisen, T. (2019). Ablation studies in artificial neural networks, *arXiv preprint arXiv:1901.08644* .

Motin, M. A., Karmakar, C. K. & Palaniswami, M. (2016). An EEMD-PCA approach to extract heart rate, respiratory rate and respiratory activity from PPG signal, *2016 38th Annual International Conference of the IEEE Engineering in Medicine and Biology Society (EMBC)*, IEEE, pp. 3817–3820.

Muñoz, J. E., Gambús, P., Jensen, E. W. & Vallverdú, M. (2018). Time-frequency features for impedance cardiography signals during anesthesia using different distribution kernels, *Methods of information in medicine* **57**(S 01): e1–e9.

Muzi, M., Ebert, T. J., Tristani, F. E., Jeutter, D. C., Barney, J. A. & Smith, J. J. (1985). Determination of cardiac output using ensemble-averaged impedance cardiograms, *Journal of Applied Physiology* **58**(1): 200–205.

Naidu, S., Bagal, U. R., Pandey, P. C., Hardas, S. & Khambete, N. D. (2015). Monitoring of stroke volume through impedance cardiography using an artificial neural network, *2015 Twenty First National Conference on Communications (NCC)*, IEEE, pp. 1–6.

Naidu, S., Pandey, P. C. & Pandey, V. K. (2011). Automatic detection of characteristic points in impedance cardiogram, *Computing in Cardiology*.

Ngui, W. K., Leong, M. S., Hee, L. M. & Abdelrhman, A. M. (2013). Wavelet analysis: Mother wavelet selection methods, *Applied Mechanics & Materials* **393**(393 (2013)): 953–958.

Pandey, V. K. & Pandey, P. C. (2007). Wavelet based cancellation of respiratory artifacts in impedance cardiography, *2007 15th International Conference on Digital Signal Processing*, IEEE, pp. 191–194.

Raza, S., Patterson, R. & Wang, L. (1992). Filtering respiration and low-frequency movement artefacts from the cardiogenic electrical impedance signal, *Medical and Biological Engineering and Computing* **30**(5): 556–561.

Revzin, M. V., Imanzadeh, A., Menias, C., Pourjabbar, S. & Pellerito, J. S. (2017). Clinical monitoring of cardiac output assessed by transoesophageal echocardiography in anaesthetised dogs: a comparison with the thermodilution technique, *BMC Veterinary Research* **13**(325): 1746–6148.

Revzin, M. V., Imanzadeh, A., Menias, C., Pourjabbar, S. & Pellerito, J. S. (2019). Optimizing image quality when evaluating blood flow at doppler us: A tutorial, *Radiographics* **39**(5): 180055.

Riese, H., Groot, P. F., van den Berg, M., Kupper, N. H., Magnee, E. H., Rohaan, E. J., Vrijkotte, T. G., Willemsen, G. & de Geus, E. J. (2003). Large-scale ensemble averaging of ambulatory impedance cardiograms, *Behavior Research Methods, Instruments, & Computers* **35**(3): 467–477.

Rosell, J., Cohen, K. P. & Webster, J. G. (1995). Reduction of motion artifacts using a two-frequency impedance plethysmograph and adaptive filtering, *IEEE Transactions on Biomedical Engineering* **42**(10): 1044–1048.

Sebastian, T., Pandey, P. C., Naidu, S. & Pandey, V. K. (2011). Wavelet based denoising for suppression of respiratory and motion artifacts in impedance cardiography, *2011 Computing in Cardiology*, IEEE, pp. 501–504.

Sheikh, S.-a. A., Shah, A., Levantsevych, O., Soudan, M., Alkhalaf, J., Rad, A. B., Inan, O. T. & Clifford, G. D. (2020). An open-source automated algorithm for removal of noisy beats for accurate impedance cardiogram analysis, *Physiological Measurement* **41**(7): 075002.

Sherwood, A., Allen, M. T., Fahrenberg, J., Kelsey, R. M., Lovallo, W. R. & Van Doornen, L. J. (1990). Methodological guidelines for impedance cardiography, *Psychophysiology* **27**(1): 1–23.

Stepanov, R., Podtaev, S., Frick, P. & Dumler, A. (2017). Beat-to-beat cardiovascular hemodynamic parameters based on wavelet spectrogram of impedance data, *Biomedical Signal Processing and Control* **36**: 50–56.

Sweeney, K. T., McLoone, S. F. & Ward, T. E. (2012). The use of ensemble empirical mode decomposition with canonical correlation analysis as a novel artifact removal technique, *IEEE Transactions on Biomedical Engineering* **60**(1): 97–105.

Tariqul Islam, M., Ahmed, T., Shahnaz, C., Anowarul Fattah, S. et al. (2018). SPECMAR: Fast heart rate estimation from PPG signal using a modified spectral subtraction scheme with composite motion artifacts reference generation, *arXiv e-prints* pp. arXiv–1810.

Wu, Z. & Huang, N. E. (2009). Ensemble empirical mode decomposition: a noise-assisted data analysis method, *Advances in Adaptive Data Analysis* **1**(01): 1–41.

Yakimets, J. & Jensen, L. (1995). Evaluation of impedance cardiography: comparison of NCCOM3-R7 with Fick and thermodilution methods, *Heart & Lung* **24**(3): 194–206.

Yamamoto, Y., Mokushi, K., Tamura, S., Mutoh, Y., Miyashita, M. & Hamamoto, H. (1988). Design and implementation of a digital filter for beat-by-beat impedance cardiography, *IEEE Transactions on Biomedical Engineering* **35**(12): 1086–1090.

Zhang, Y., Qu, M., Webster, J. G., Tompkins, W. J., Ward, B. A. & Bassett, D. R. (2007). Cardiac output monitoring by impedance cardiography during treadmill exercise, *IEEE Transactions on Biomedical Engineering* **BME-33**(11): 1037–1042.

Zhang, Z., Pi, Z. & Liu, B. (2014). Troika: A general framework for heart rate monitoring using wrist-type photoplethysmographic signals during intensive physical exercise, *IEEE Transactions on*

Biomedical Engineering **62**(2): 522–531.